Fuel Droplet Burning Rates at High Pressures

by

G. S. Canada and G. M. Faeth
Department of Mechanical Engineering
The Pennsylvania State University
University Park, Pennsylvania

Combustion of methanol, ethanol, propanol -1, n - pentane, n - heptane and n - decane was observed in air under natural convection conditions at pressures up to 100 atm. The droplets were simulated by porous spheres with diameters in the range 0.63 - 1.90 cm. The pressure levels of the tests were high enough so that near critical combustion was observed for methanol and ethanol. Measurements were made of the burning rate and liquid surface temperatures of the fuels. The data were compared with variable property analysis of the combustion process, including a correction for natural convection. Due to the high pressures, the phase equilibrium models of the analysis included both the conventional low pressure approach as well as high pressure versions allowing for real gas effects and the solubility of combustion product gases in the liquid phase. The burning rate predictions of the various theories were similar and in fair agreement with the data. The high pressure theory gave the best prediction for the liquid surface temperatures of ethanol and propanol -1 at high pressure. The experiments indicated the approach of critical burning conditions for methanol and ethanol at pressures on the order of 80 - 100 atm, which was in good agreement with the predictions of both the low and high pressure analysis.

Critical burning conditions could not be approached for the remaining fuels due to the formation of soot deposites on the sphere at pressures in the range 30 - 60 atm.

Introduction

In recent years, there has been increased interest in droplet processes at elevated pressures where the droplet can approach or exceed its critical point during combustion.[1-4] Once the droplet exceeds its critical point the fuel is gasified and the droplet burning rate is no longer controlled by the evaporation of the fuel. In this range of conditions, the combustion process proceeds as an unsteady diffusion flame until all the fuel vapor is consumed. This type of combustion behavior has been observed experimentally by Faeth, et al.[5]

Differences in the gasification mechanism have also been encountered when a droplet approaches, but does not exceed, its critical point. For droplet evaporation at low ambient temperatures and high pressures, Manrique and Borman[6] and Savory and Borman[7] found appreciable quantities of the ambient gas dissolved in the liquid phase in the near - critical regime. In this case, dissolved gases and other real gas effects combined to influence gasification rates as well as the conditions required to approach the critical point. Real gas effects have also been found to influence the conditions required for critical droplet combustion.[8]

While measurements have been made of high pressure droplet evaporation rates,[7,9] comparable data are not available for droplet combustion. Hall and Diederichsen[10] studied the combustion of suspended droplets in air at pressures up to 20 atm, however, the data is presented as total droplet lifetime (which includes both heat - up and quasi - steady burning) which complicates the interpretation of these results. Furthermore, the pressure level of these experiments is not high enough to illustrate high pressure effects to a significant degree.

Brzustowski and Natarajan[11], present similar total lifetime data for aniline at pressures up to 55 atm. Lazar and Faeth[8], were also unable to obtain high pressure steady droplet burning rate measurements.

The present investigation emphasized the measurement of steady liquid fuel burning rates at high pressures. The experimental results were compared with droplet combustion theories which both neglected and considered real gas effects. In order to insure measurements at steady conditions, the fuel droplets were simulated by porous spheres. Combustion was observed in air, at pressures up to 100 atm, under natural convection conditions. The fuels considered in the study included methanol, ethanol, propanol -1, n - pentane, n - heptane and n - decane.

Apparatus

A sketch of the experimental apparatus in shown in Figure 1. The test chamber consisted of a high pressure cylindrical vessel, 66 cm long with an inside diameter of 13 cm. The chamber was fitted with windows to allow observation of the combustion process.

The fuel was fed to the center of the porous alundum sphere through a water cooled hypodermic tube (Figure 1). Spheres having diameters of 0.64, 0.95 and 1.90 cm were employed in the testing. The outside diameter of the coolant tube was 0.20 cm for the 0.64 cm diameter sphere and 0.32 cm for the larger spheres. The fuel flow rate was controlled by a variable displacement diaphragm pump and measured with a system of graduated burets at the pump inlet. The steady burning rate was determined as the flow rate where the surface of the sphere was fully wetted and not dripping. During adjustment to the steady burning condition, fuel dripping from the sphere was collected in a dead-ended tube at the bottom of the apparatus. The sphere was ignited

by momentarily placing it in the vicinity of a electrically heated wire.

Liquid surface temperatures were measured during tests with the 0.95 cm diameter sphere. These measurements were made with two 0.005 cm diameter chromel - alumel thermocouples mounted on opposite sides of the surface of the sphere, 60^{o} from the bottom stagnation point.

A constant gas composition was maintained around the sphere by adding air through a manifold at the bottom of the chamber. The drift velocity of the air past the position of the sphere, however, was sufficiently low so that natural convection was the predominant convection effect. The exhaust gas was removed from the top of the chamber through a water cooled tube. After cooling and trapping out condensate, the exhaust gas was passed through a needle valve which controlled the pressure of the test chamber.

Theory

In many respects, the present theory is similar to that of Refs. 8 and 12 for high pressure droplet combustion, therefore, only a brief discussion of the analysis will be undertaken in the following. The major point of difference involves the different boundary conditions at the liquid surface for the present porous sphere combustion as opposed to steady droplet combustion.

The theory may be divided into a gas phase model of the combustion process and a phase equilibrium model for conditions at the liquid surface. In the gas phase model, the effect of convection is treated by the usual multiplicative correction of the burning rate predicted in the absence of convection.[13,14] Therefore, the basic analysis assumes spherical symmetry and neglects convection effects. The remaining assumptions are similar to those of Refs. 8, 12 and 13. The

reaction is taken to be confined to an infinitely thin flame surface, where fuel and oxidizer combine in a stoichiometric proportions. The process is assumed to be steady, dissociation and radiation are neglected and the total pressure is assumed to be uniform throughout the system.

Only concentration diffusion is considered in the gas phase analysis and the influence of compressibility on transport properties is neglected. The concentration dependence of the thermal conductivity is neglected and the binary diffusivities of all species are taken to be the same, although different values of each of these properties can be employed inside and outside the flame. Since earlier studies have shown that the value of the Lewis number has a strong influence on conditions at the liquid surface,[8] the common unity Lewis number assumption was not employed in the analysis.

In the present experiment, the liquid fuel was pumped from a storage vessel at atmospheric pressure to the center of the sphere. Therefore, due to the low solubility of gases in the test fuels at low pressures, it is appropriate to assume that the liquid entering the sphere has a negligible dissolved gas concentration. Under this assumption, the liquid phase flux of dissolved gas is zero and the fuel is the only component with a finite molar flux inside the flame surface.

The specific heat of each species was assumed to be a linear function of temperature

$$C_{pi} = a_i + b_i T. \qquad (1)$$

The thermal conductivity was also assumed to be proportional to temperature in the regions inside and outside the flame

$$\lambda = \lambda_s (T/T_s). \qquad (2)$$

The quantity

$$\chi = \lambda/(cD) \qquad (3)$$

is only a weak function of temperature and composition and was assumed to be a constant inside and outside the flame.

With due allowance for the fact that the fuel mole flux fraction is unity in the region inside the flame, the details of the gas phase analysis are very similar to that presented in Ref. 12. The specific results obtained in the present case are given in the appendix. In addition to this variable property - variable specific heat analysis, calculations were also performed for variable property - constant specific heat and constant property models.

The semi-empirical correction, for the effect of natural convection on the burning rate,[14] was based on the natural convection heat transfer correlation determined by Yuge.[15] In addition, the Grashoff number for burning spheres suggested by Spalding[16] was employed in the correlation. The specific equation used in the calculations is as follows

$$\frac{\dot{m}}{\dot{m}_o} = 1 + 0.221\ Pr^{1/3}(d^3 g/\nu^2)^{1/4} \qquad (4)$$

In order to avoid ambiguity, the properties used in this correlation were taken at the ambient conditions of the burning sphere.

Three models were employed for computing phase equilibrium at the liquid surface. The simplest model (low pressure theory) neglected the solubility of the product gases in the liquid phase and other high pressure corrections. The fuel mole fraction at the liquid surface was taken to be the vapor pressure of the pure fuel, at

the surface temperature, divided by the total pressure. The total enthalpy rise of vaporization, L_1, was determined by summing the compressed liquid enthalpy change at T_o, the heat of vaporization at T_o, the ideal gas enthalpyriso between T_o and T_s and the enthalpy deviations between saturated vapor and the ideal gas states at T_o and T_s. In this case, the ideal gas enthalpy rise was computed by integrating actual specific heat correlations between T_o and T_s, as opposed to the linearized specific heat correlation (Eq. 1) employed in the gas phase analysis. The enthalpy deviations were obtained from the tables of Lyderson, et al, presented in Ref. 17.

The high-pressure theories considered solubility and other high-pressure effects through the use of a modified Redlick-Kwong equation of state with mixing rules given by Prausnitz and Chueh.[18] For combustion in air, the major gaseous species at the liquid surface are fuel vapor, nitrogen, carbon dioxide and water vapor. Since nitrogen predominates the non-fuel gases in this system, the simplified version of the high pressure theory assumed that this system could be represented by a binary mixture of fuel and nitrogen. The more complete version of the high pressure theory considered the complete quaternary system; fuel, nitrogen, carbon dioxide and water.

The details of the formulation of the high pressure phase equilibrium model are given in Ref. 12. The dimensionless constants required by the Redlick-Kwong equation of state were obtained by setting the first and second isothermal derivatives of pressure, with respect to volume, equal to zero at the critical point. The binary interaction parameters, k_{ij}, required by the theory are listed in Ref. 8 for the paraffins and the combustion product gases. For the alcohols,

the k_{ij} values were taken to be the same as that of the hydrocarbon homomorph of fuel. These values are listed in Table 1. For the high pressure theories, the enthalpy deviations required in the calculation of the total heat of vaporization of the fuel were computed directly from the Redlick-Kwong equation of state. The remaining terms comprising the enthalpy rise of vaporization were computed in the same manner as in the low pressure theory calculations.

The sources of property data and correlations were the same as in earlier studies.[8,12,13] The particular values employed in the present calculations are given in Table II (with the exception of L_1 which is too variable to be represented by a single value). The calculations proceeded by guessing a value for the liquid surface temperature T_s, at a given total pressure, and then computing L_1 and X_{Is} (the fuel mole fraction at the liquid surface) from the phase equilibrium analysis. These values of L_1 and T_s were then employed to compute a value for X_{1s} from the gas phase analysis (eq. A-1 to A-13). The final solution was obtained by varying T_s until the two values of X_{1s} were matched.

Results and Discussion

All the experimental results were obtained for combustion in air. The ambient air temperature and the fuel inlet temperature were both 300 K. The 0.95 cm diam sphere was used for the bulk of the burning rate measurements. Figures 2 and 3 illustrate the results for the alcohols and paraffins, respectively.

The theoretical results shown in Figures 2 and 3 were calculated with the variable property - variable specific heat gas phase analysis. The quaternary version is illustrated for the high-pressure theory. The theoretical curves are terminated at high pressures when the critical

burning condition is reached. For the low-pressure theory, critical burning was assumed when the liquid surface temperature was equal to the critical temperature of the fuel. Critical burning for the high-pressure theory formally occurs when the liquid surface reaches its critical mixing point for the conditions of the combustion process. The burning rate predictions of the two theories are almost identical, although the high pressure theory generally predicts a higher pressure for critical combustion.

The experimental results for methanol and ethanol (Figure 2) were terminated at high pressures due to difficulties in determining the burning rate. At pressures on the order of 80-100 atm, for these fuels, the flame zone would tend to move away from the sphere with increased fuel flow rates, and clear evidence of fuel dripping could not be obtained. This behavior probably indicates the onset of critical burning for these fuels, although the pressure where this occured could not be defined very precisely.

The burning rate data for the remaining fuels in Figures 2 and 3 are terminated at high pressures due to the formation of soot. In these cases, carbon spots would form and grow on the surface of the sphere causing the test to be terminated at elevated pressures.

The absolute agreement between the theoretical and experimental burning rates in Figures 2 and 3 is comparable to results obtained in low pressure tests, e.g. Ref. 13. In particular, the theory gives a reasonably good indication of the rate of increase of the burning rate with increasing pressure.

The effect of varying sphere size is examined for n - heptane and methanol in Figure 4. For this plot, the dimensionless burning rate, normalized by the convection correction, is employed for the ordinate so that the data for various sphere sizes should fall

on a single curve. It is seen that this normalized burning rate (which corresponds to the no-convection burning rate of the theory) is almost a constant up to the critical burning condition for the present porous sphere experiments. This is due to the fact that the no-convection burning rate is largely dependent upon the total enthalpy rise of vaporization, which does not change to a great degree with increasing pressure for porous spheres. In this case, the reduced heat of vaporization near the critical point is compensated by increases in the enthalpy rise required to bring the fuel from the inlet to the surface temperature.

The fact that the normalized burning rate is relatively constant indicates that the increase in burning rate with increasing pressure in Figures 2 and 3 is largely due to convection effects. The present experimental results represent a reasonably good test of the burning rate correction for natural convection, since the Grashoff number, based on the Spalding definition used in (Eq. 1), varies in the range 10^4 - 10^8.

The liquid surface temperature results for the six fuels are illustrated in Figures 5 and 6. The boiling point curves and the surface temperature predictions of both the low-pressure and quaternary high-pressure theories are shown on the figures along with the data. The difference between the two theories is more obvious with regard to surface temperatures, than was the case for burning rates, with the high pressure theory predicting the lowest surface temperature at a given pressure.

It is seen in Figure 5 that the data for ethanol and propanol -1 agrees reasonably well with the high pressure theory at high pressures. For methanol, however, the low pressure theory gives the best estimation of the data over the entire test range. The poorer high-pressure theoretical results for methanol could be due to the large quantities of water vapor

in the combustion products of this fuel. Water is difficult to model precisely in the high-pressure phase equilibrium analysis, and materials with high water vapor concentrations in the products have generally shown poorer agreement with the high-pressure theory in the past.[19] The data for the paraffins in Figure 6 could not be extended to sufficiently high pressures to provide an adequate test of high pressure theory due to the soot formation. Over the available experimental range, the low pressure theory appears to be adequate for these materials.

Figure 7 illustrates computed gas and liquid phase compositions, at the liquid surface, for ethanol and n-heptane. These results pertain to porous sphere combustion in air, with a fuel inlet and ambient air temperature of 300 K. The gas phase composition remains relatively constant as the total pressure is increased for both fuels. In contrast, the liquid phase concentration of dissolved gas increases significantly with increasing pressure. The critical mixing point of the surface (the critical combustion condition) is indicated by the equality of the liquid and gas phase composition at this state. The dissolved gas concentration becomes quite large near the critical combustion condition for the present test conditions, reaching values as high as 60% for n decane.

At pressures higher than the critical combustion condition, the process is similar to the porous sphere combustion of gas. In this regime, no liquid surface would be observed and a range of fuel flow rates (subject to blow-off and quenching limits) could be accomodated by the sphere at a given pressure; as opposed to the single fuel flow rate possible for liquid fuel combustion at pressures below the critical combustion condition.

The previous high pressure theoretical results were obtained with the quaternary phase equilibrium model. The simplified binary model

gave essentially the same results with regard to burning rates and liquid surface temperatures. In contrast to high pressure droplet combustion,[8] however, there were significant differences between the critical porous sphere combustion pressures predicted by the two high-pressure theories. The critical combustion conditions for all three theories are compared with pure fuel critical properties in Table III. In agreement with the experimental findings, both the low pressure and high pressure quaternary theories predict critical burning pressures on the order of 100 atm for methanol and ethanol. The theoretical indication that ethanol should experience critical burning at pressures somewhat below methanol is also in qualitative agreement with the fact that experimental difficulities in determining burning rates were encountered at somewhat lower pressures for ethanol, c.f. Figure 2.

All the previous theoretical results were obtained with the variable property - variable specific heat gas phase analysis, using the properties listed in Table II. The use of the variable property-constant specific heat and constant property gas phase analysis gave essentially the same results, when the respective constant properties in each of these cases were evaluated at average conditions in each region. The effect of parametric variations of the k_{ij} and the gas phase properties listed in Table II was also examined. The value of χ_i had the greatest influence on the prediction of liquid surface temperatures and critical burning conditions. Quantitatively, the effect of variations of this parameter was similar to that encountered in earlier studies of high pressure combustion.[13,19] Variations in the predicted burning rates were almost in direct proportion to variations in the value of λ_i, and were relatively insensitive to changes in χ_i.

Conclusions

The low and high pressure theories gave essentially the same prediction of burning rates at high pressures. The discrepancies between theory and experiment over the present test range were comparable to the errors encountered in earlier studies at atmospheric pressure.[13] The convection correction given in Eq. (1) gave reasonably good results for Grashoff numbers in the range 10^4 - 10^8.

The greatest differences between the theories were encountered in the prediction of liquid surface temperatures and critical burning conditions. The quaternary high pressure theory gave the best agreement with the experimental results for ethanol and propanol -1. The low pressure theory, however, was superior for methanol. It is suggested that the greater amount of water vapor in the combustion products of methanol is responsible for the poorer agreement of the high-pressure theory for this fuel. The experimental results for the paraffins did not extend to high enough pressures to provide a test of the high pressure theory.

The experiments indicated that the methanol and ethanol were approaching critical combustion conditions at pressures on the order of 80 - 100 atm. Both the low pressure and high pressure quaternary theories predicted critical burning in reasonable agreement with these results. Critical burning conditions could not be approached for the remaining fuels due to the formation of soot deposites on the sphere at pressures in the range 30 - 60 atm.

The use of variable property - variable specific heat, variable property - constant specific heat and constant property gas phase analyses gave essentially the same results as long as the respective constant properties were evaluated at average conditions inside and

outside the flame. Parametric property variations caused variations in the computed results similar to those encountered in earlier high pressure combustion studies.[8,13,19] For porous spheres, the binary high pressure theory gave a poorer approximation of the quaternary high-pressure theory, than was the case for high pressure droplet combustion.[8]

Nomenclature

a_i, b_i	specific heat parameters, Eq.(1)
a', b'	weighted specific heat parameters, Eq.(A-11)
c	concentration
C_p	specific heat
d	droplet diameter
D	binary diffusivity
g	acceleration of gravity
L	enthalpy rise of vaporization
$\dot{n}$	total molar flow rate
Pr	Prandtl number
Q_s	enthalpy of reaction
r	radial distance
T	temperature
X	mole fraction
α_i	stoichiometry parameter, Eq.(A-6)
α'	weighted stoichiometry parameter, Eq.(A-8)
λ	thermal conductivity
ν	kinematic viscosity
ξ,ξ'	parameters, Eqs.(A-2) and (A-10)
ϕ,ϕ'	parameters, Eqs.(A-2) and (A-10)
χ	parameter, Eq.3

Subscripts

c	flame surface
e	region outside flame
i	region inside flame
o	no convection condition
s	liquid surface
∞	ambient conditions

Appendix

In the following, the fuel is denoted as component 1 and oxygen is denoted as component n. The gas phase solution in the region inside the flame gives the following expression for the fuel mole fraction at the liquid surface

$$X_{1s} = 1 - \left[\frac{(a_1 + b_1T_c + \xi)(a_1 + b_1T_s - \xi)}{(a_1 + b_1T_c - \xi)(a_1 + b_1T_s + \xi)}\right]^{\chi_i/\xi} \quad ,\xi^2>o \qquad (A\text{-}1)$$

where

$$\xi^2 = -\phi^2 = a_1^2 - 2b_1\left(L_1 - a_1T_s - \frac{b_1}{2}T_s^2\right) \qquad (A\text{-}2)$$

The solution has a second branch for negative values of ξ^2,

$$X_{1s} = 1 - \exp\left\{\frac{2\chi_i}{\phi}\left[\tan^{-1}\left(\frac{a_1 + b_1T_s}{\phi}\right) - \tan^{-1}\left(\frac{a_1 + b_1T_c}{\phi}\right)\right]\right\}, \quad \phi^2>o \qquad (A\text{-}3)$$

The mole fractions of the remaining species at the liquid surface are given in terms of the composition of the flame

$$X_{js} = X_{jc}\,(1-X_{1s}) \;, \quad j=2,\ldots,n-1 \qquad (A\text{-}4)$$

The solution in the region inside the flame also yields an expression for the burning rate in terms of properties in the flame

$$\frac{\dot{n}_o T_s b_1}{4\pi r_s \lambda_{s_i}}\left(1 - \frac{r_s}{r_c}\right) = \ln\left\{\left[1 + \frac{a_1}{L_1}(T_c - T_s) + \frac{b_1}{2L_1}(T_c^2 - T_s^2)\right](1-X_{1s})^{a_1/\chi_i}\right\} \qquad (A\text{-}5)$$

The stoichiometry of the reaction is taken as follows

$$M_1 \rightarrow \sum_{j=2}^{n} \alpha_j M_j \qquad (A\text{-}6)$$

The concentration of fuel and oxygen is zero in the flame. The solution in the region outside the flame yields the following expression for the composition of the remaining species in the flame

$$(\alpha' X_{jc} - \alpha_j)/(\alpha' X_{j\infty} - \alpha_j) = \alpha_n/(\alpha_n - \alpha' X_{n\infty}) \qquad \text{(A-7)}$$

where

$$\alpha' = \sum_{j=2}^{n} \alpha_j \qquad \text{(A-8)}$$

The flame temperature is related to the ambient oxygen concentration as follows

$$\frac{(a'+b'T_\infty+\xi')(a'+b'T_c-\xi')}{(a'+b'T_\infty-\xi')(a'+b'T_c+\xi')} = \left(\frac{\alpha_n}{\alpha_n-\alpha' X_{n\infty}}\right)^{\sqrt{\frac{\alpha' \chi_e}{\xi'}}}, \quad \xi'^2>0 \qquad \text{(A-9)}$$

where

$$\xi'^2 = -\phi'^2 = a'^2 - 2b'\left(L_1 - Q_s - a'T_s - \frac{b'}{2}T_s^2\right). \qquad \text{(A-10)}$$

In these equations, Q_s is the enthalpy of reaction of gaseous fuel and products at T_s and

$$a' = \sum_{j=2}^{n} \alpha_j a_j \quad , \quad b' = \sum_{j=2}^{n} \alpha_j b_j \qquad \text{(A-11)}$$

The other branch of the solution is

$$\exp\left\{\tan^{-1}\left(\frac{a'+b'T_c}{\phi'}\right) - \tan^{-1}\left(\frac{a'+b'T_\infty}{\phi'}\right)\right\} = \left(\frac{\alpha_n}{\alpha_n-\alpha' X_{n\infty}}\right)^{\sqrt{\frac{2\alpha' \chi_e}{\phi'}}}, \quad \phi'^2>0 \qquad \text{(A-12)}$$

The solution in the region outside the flame also yields an expression relating the burning rate to properties in the flame

$$\frac{\dot{n}_o T_s b'}{4\pi r_c \lambda_{se}} = \ln \left\{ \left[\frac{L_1 - Q_s + a'(T_\infty - T_s) + \frac{b'}{2}(T_\infty^2 - T_s^2)}{L_1 - Q_s + a'(T_c - T_s) + \frac{b'}{2}(T_c^2 - T_s^2)} \right] \left(\frac{\alpha_n}{\alpha_n - \alpha' X_{n\infty}} \right)^{\frac{a'}{\alpha' X_e}} \right\} \qquad \text{(A-13)}$$

Given T_s, T_∞ and the ambient compostion, Eqs. (A-1) - (A-13) are sufficient to solve for T_c, $\dot{n}_o$, r_c and the composition of the flame and the liquid surface.

Acknowledgments

This work was sponsored by the National Aeronautics and Space Administration, Grant NGR 39-009-077, under the technical management of R. J. Priem of the Lewis Research Center. The authors also wish to thank R. S. Lazar for his assistance with the phase equilibrium calculations.

References

1. Spalding, D. B. : ARS J 29, 828 (1959).

2. Wieber, P. R. : AIAA J 1,2764 (1963).

3. Brzustowski, T. A. : Can. J. Chem Eng. 43,30 (1965).

4. Rosner, D. E. : AIAA J 5,163 (1967).

5. Faeth, G. M., et al, : Twelfth Symposium (International) on Combustion, p.9, The Combustion Institute, 1969.

6. Manrique, J. A. and Borman, G. L. : Intern. J. Heat Mass Transfer 12,1081 (1969).

7. Savory, W. and Borman, G. L. : "Experiments on Droplet Vaporization at Supercritical Pressures," AIAA Paper No. 70-6, 1970.

8. Lazar, R. S. and Faeth, G. M. : Thirteenth Symposium (International) on Combustion, p.801, The Combustion Institute, 1971.

9. Torda, T. P. and Matlosz, R. : "Liquid Droplet Evaporation in a Stagnant High Pressure and High Temperature Environment," NASA CR-72373, 1968.

10. Hall, A. R. and Diederichsen, J. : Fourth Symposium (International) on Combustion, p.837, Williams and Wilkins, 1953.

11. Brzustowski, T. A. and Natarajan, R. : Can. J. Chem. Eng. 44,194 (1966).

12. Lazar, R. S. : "Bipropellant Droplet Combustion in the Vicinity of the Critical Point." Ph.D. Thesis, The Pennsylvania State University, 1970.

13. Faeth, G. M. and Lazar, R. S. : AIAA J 9,2165 (1971).

14. Williams, F. A. : Combustion Theory, p.56, Addison-Wesley, 1965.

15. Yuge, T. : Trans. Am. Soc. Mech. Engrs. 82C, 214 (1960).

16. Spalding, D. B. : Fourth Symposium (International) on Combustion, p.847, Williams and Wilkins, 1953.

17. Reid, R. C. and Sherwood, T. K. : The Properties of Gases and Liquids, 2nd Edition, p.596, McGraw-Hill, 1966.

18. Prausnitz, J. M. and Chueh, P. L.: Computer Calculations for High Pressure Vapor-Liquid Equilibria, p.18, Prentice-Hall, 1968.

19. Faeth, G. M. : Combustion and Flame 18,103 (1972)

Table I

Alcohol binary interaction parameters, k_{ij}

Substance	N_2	CO_2	H_2O
methanol	.10	.08	.15
ethanol	.15	.11	.20
propanol -1	.20	.16	.25

Note: $k_{ij} = k_{ji}$ and $k_{ii} = 0$

Table II

Properties used in the gas phase calculations.

Material	a cal/gmol K	b cal/gmol K^2	$\lambda_i x10^{4*}$ cal/sec cm K	$\lambda_e x10^{4*}$ cal/sec cm K	χ_i cal/gmol K	χ_e cal/gmol K	$Q_s^{\dagger}$ K cal/gmol
Methanol	11.0	0.009	2.26	1.64	14.0	8.29	161.7
Ethanol	17.6	0.013	2.22	1.61	19.2	8.60	305.5
Propanol -1	22.0	0.019	2.17	1.59	21.8	8.20	452.2
n-pentane	31.8	0.029	1.78	1.57	21.9	8.17	782.0
n-heptane	44.1	0.040	1.72	1.57	23.6	8.17	1075.9
n-decane	62.7	0.057	1.54	1.57	28.0	8.17	1516.6
CO_2	9.0	0.0025					
H_2O	7.9	0.0018					
N_2	6.9	0.0008					
O_2	7.1	0.0010					

*at $1000^{o}K$, χ from Eq. (2) at any other temperature.

†at $298^{o}K$.

Table III

Predicted Critical Burning Conditions for Porous Sphere Combustion in Air*

Substance	CH_3OH	C_2H_5OH	C_3H_7OH	C_5H_{12}	C_7H_{16}	$C_{10}H_{22}$
Critical Properties						
Pressure	78.5	63.0	51.0	33.3	27.0	20.8
Temperature	513.2	516.0	540.7	469.5	540.2	619.0
Low Pressure Theory						
Total Pressure	109	88	78	48	52	51
Surface Temperature	513.2	516.0	540.7	469.5	540.2	619.0
Binary High Pressure Theory						
Total Pressure	168	125	125	82	108	125
Surface Temperature	489	496	516	450	512	590
Quaternary High Pressure Theory						
Total Pressure	114	100	102	65	80	108
Surface Temperature	486	494	514	449	510	583

*Fuel inlet and ambient air temperature of $300^{\circ}K$, pressure in atm, temperatures in K.

List of Figures

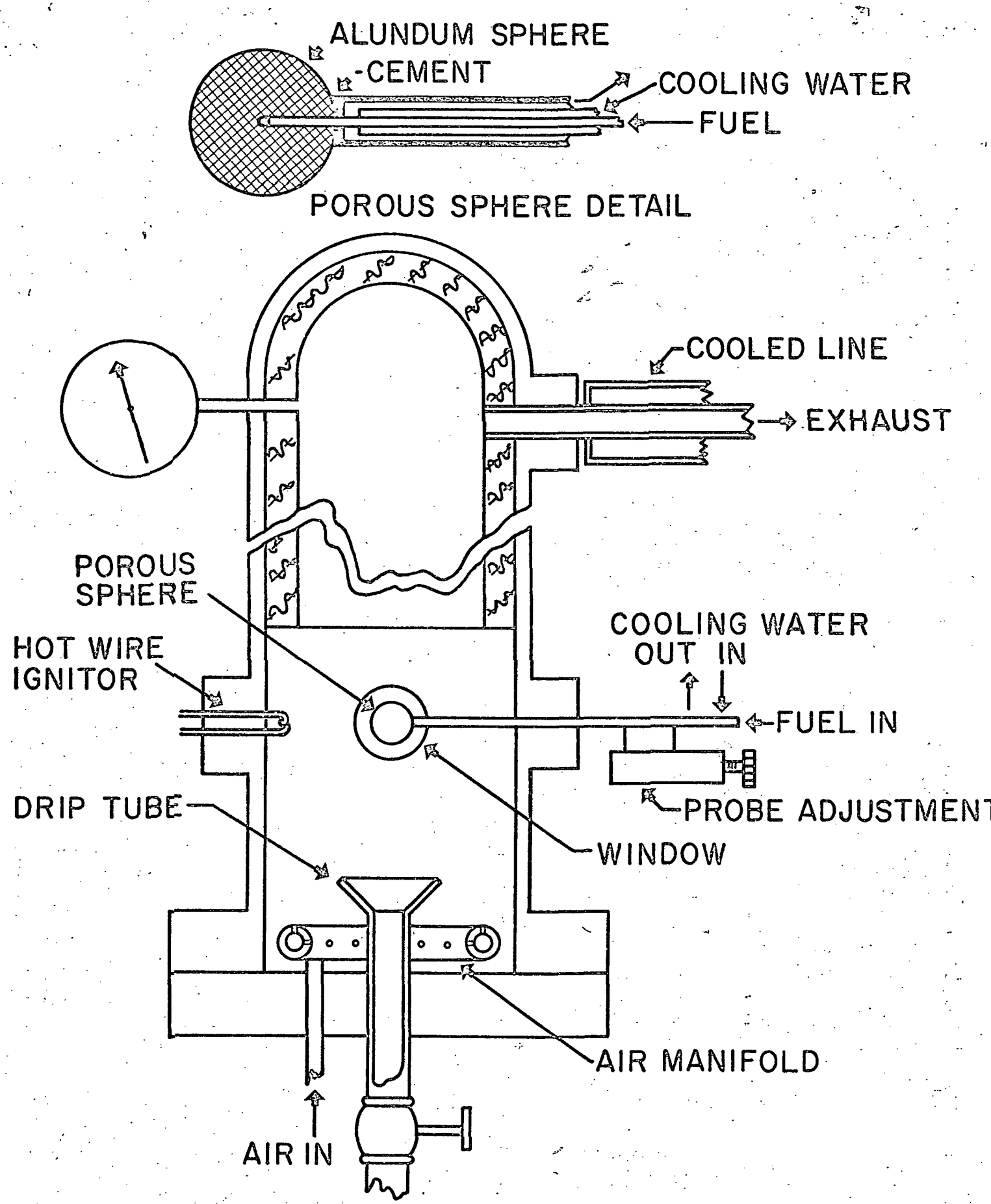
ALUNDUM SPHERE
CEMENT
COOLING WATER
FUEL
POROUS SPHERE DETAIL
COOLED LINE
EXHAUST
POROUS SPHERE
HOT WIRE IGNITOR
COOLING WATER OUT IN
FUEL IN
DRIP TUBE
PROBE ADJUSTMENT
WINDOW
AIR MANIFOLD
AIR IN

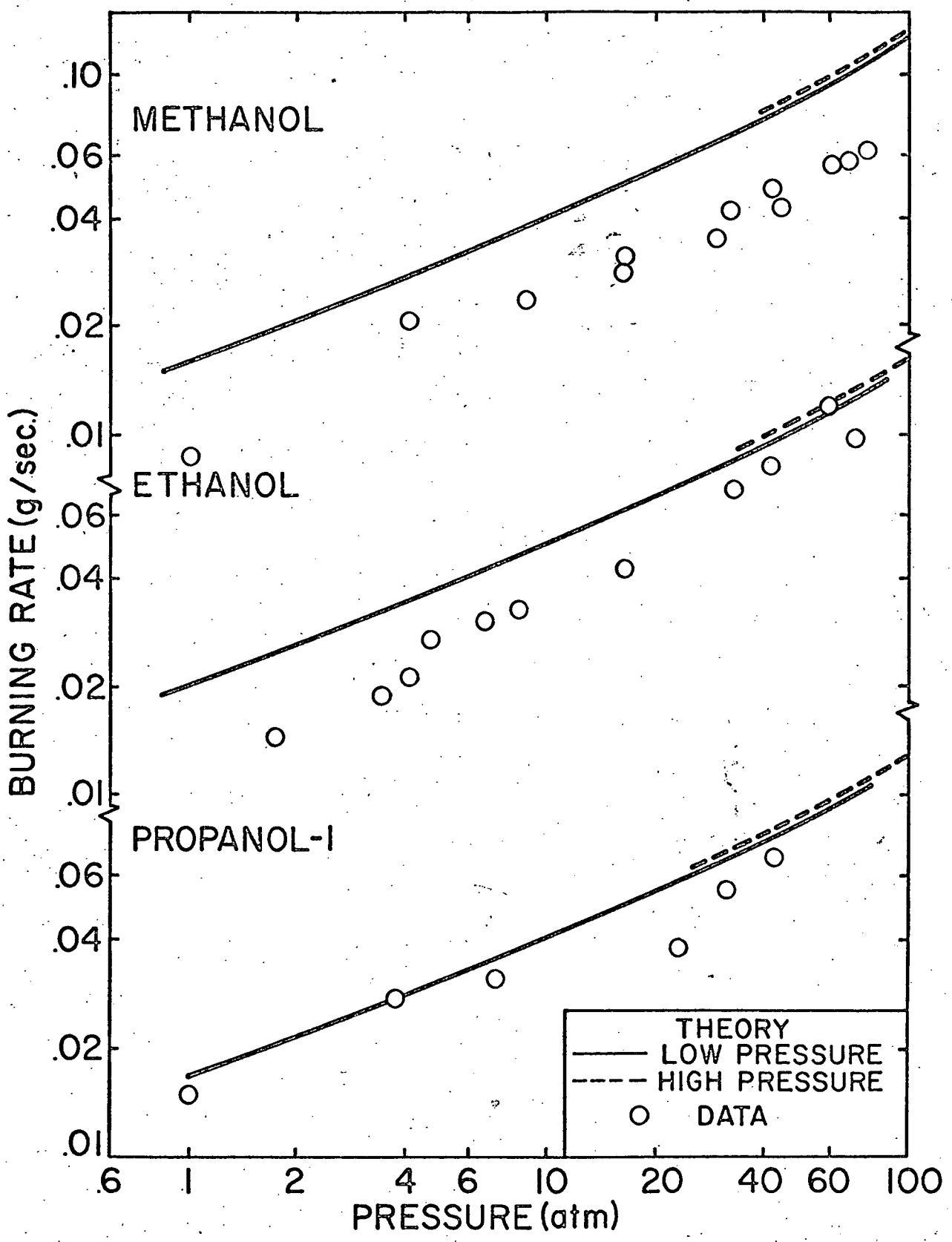
METHANOL
ETHANOL
PROPANOL-I
BURNING RATE (g/sec.)
PRESSURE (atm)
.10
.06
.04
.02
.01
.6
1
2
4
6
10
20
40
60
100
THEORY
LOW PRESSURE
HIGH PRESSURE
DATA

Fig 2

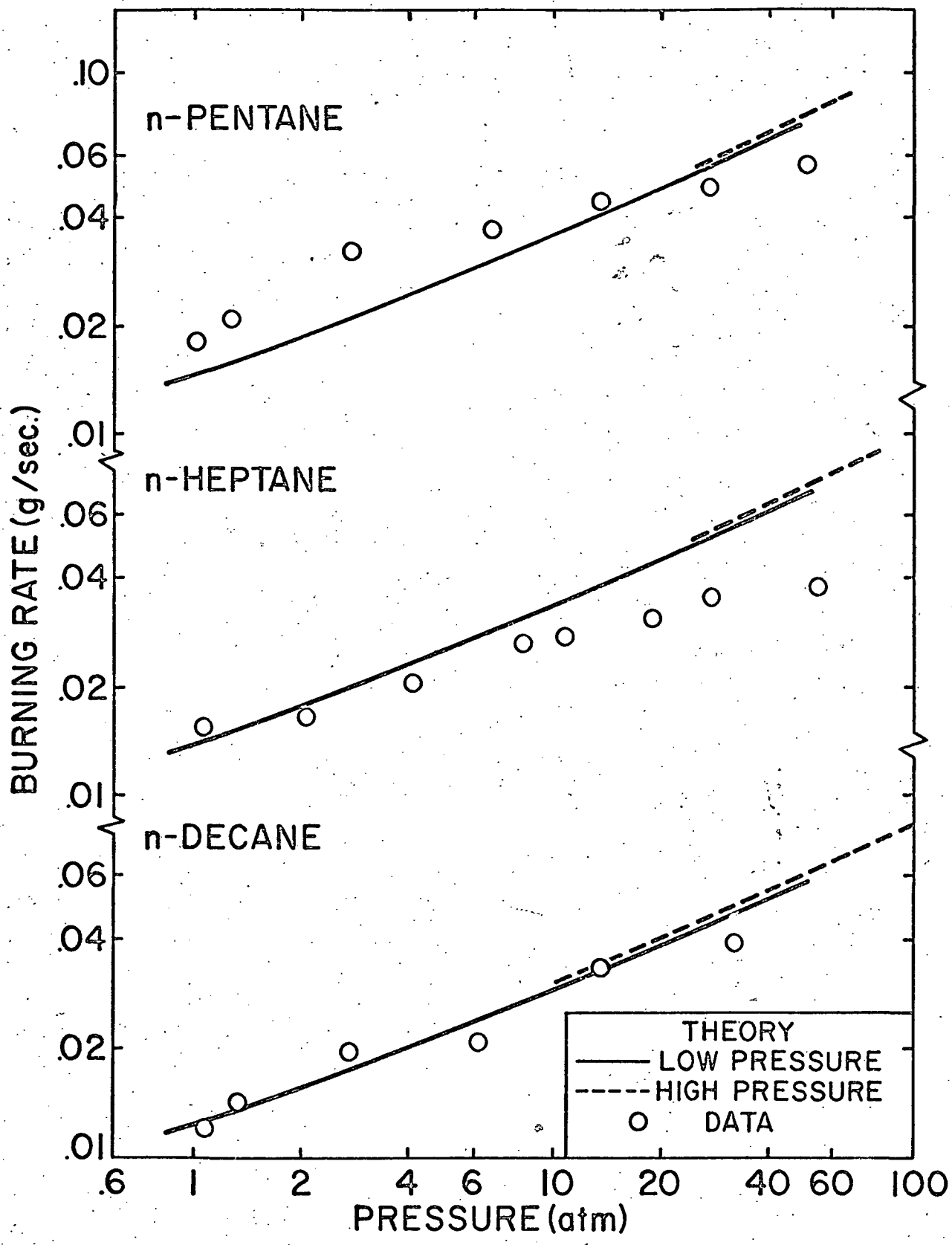
n-PENTANE
n-HEPTANE
n-DECANE
BURNING RATE (g/sec.)
.10
.06
.04
.02
.01
.6
1
2
4
6
10
20
40
60
100
PRESSURE (atm)
THEORY
LOW PRESSURE
HIGH PRESSURE
DATA

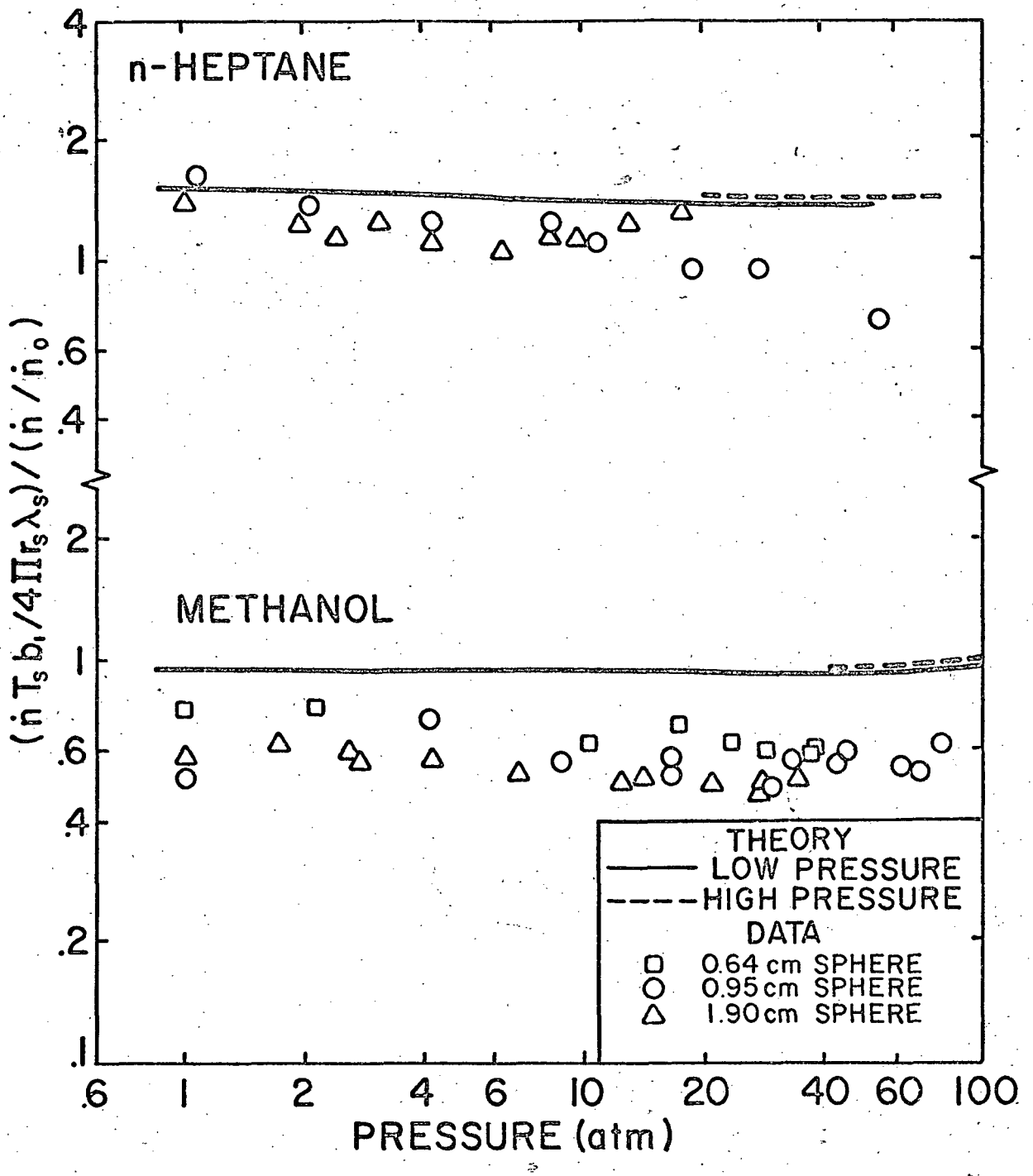
n-HEPTANE
METHANOL
$(\dot{n} T_s b_1 / 4\Pi r_s \lambda_s) / (\dot{n} / \dot{n}_o)$
PRESSURE (atm)
4
2
1
.6
.4
2
1
.6
.4
.2
.1
.6
1
2
4
6
10
20
40
60
100
THEORY
LOW PRESSURE
HIGH PRESSURE
DATA
0.64 cm SPHERE
0.95 cm SPHERE
1.90 cm SPHERE

Fig 4

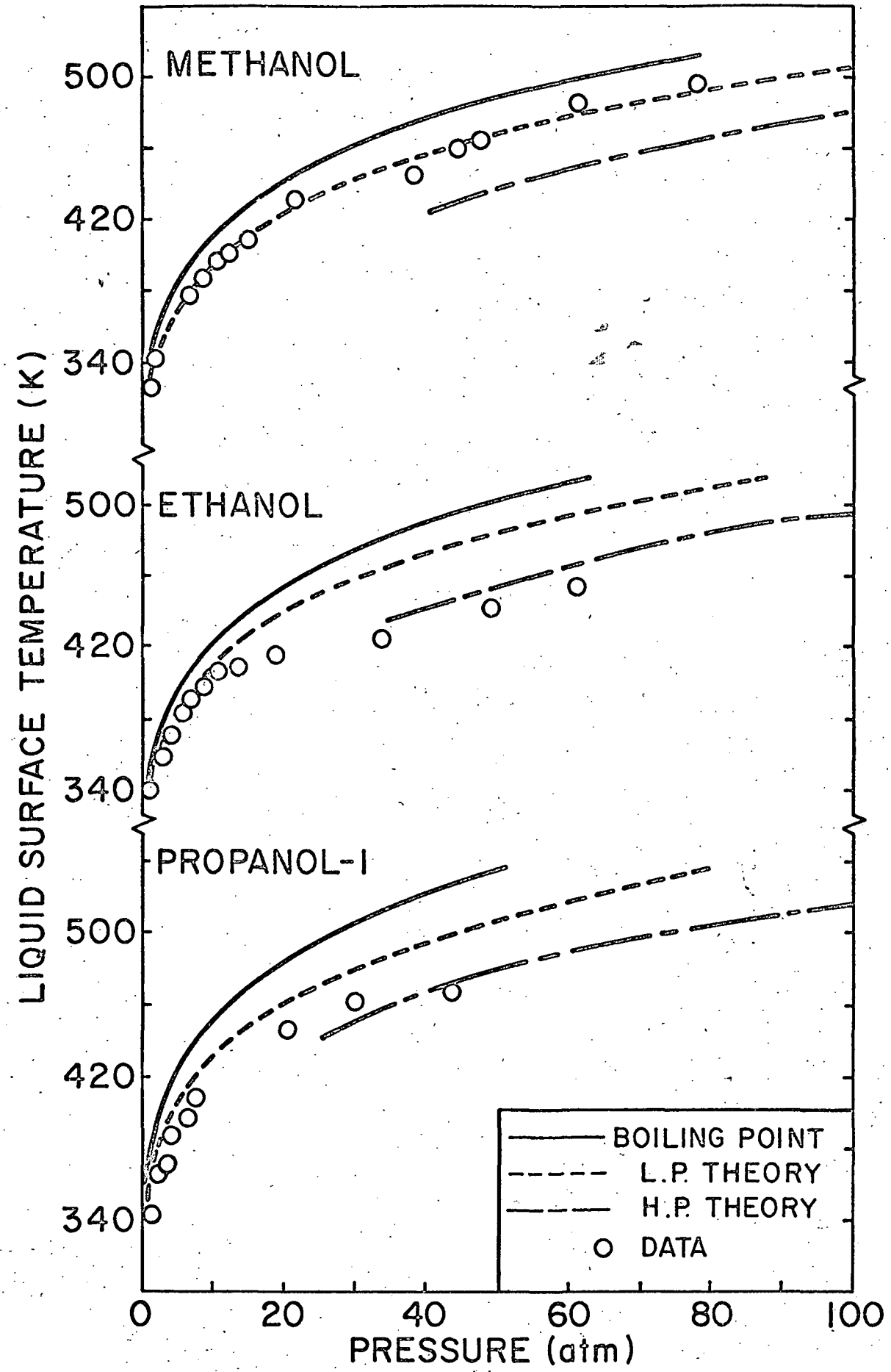
METHANOL
ETHANOL
PROPANOL-I
500
420
340
LIQUID SURFACE TEMPERATURE (K)
0
20
40
60
80
100
PRESSURE (atm)
BOILING POINT
L.P. THEORY
H.P. THEORY
DATA

Fig 5

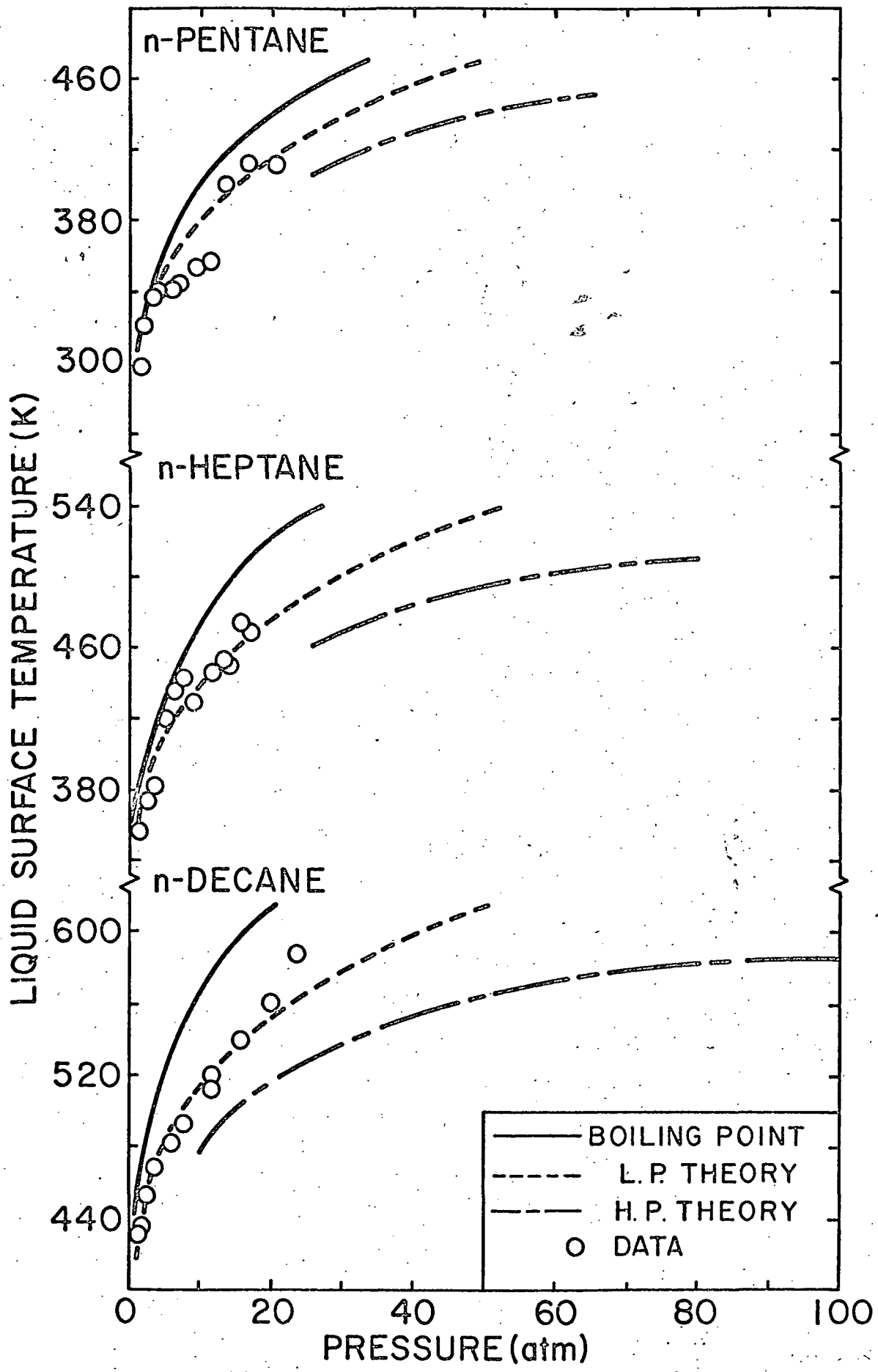
n-PENTANE
n-HEPTANE
n-DECANE
LIQUID SURFACE TEMPERATURE (K)
PRESSURE (atm)
460
380
300
540
460
380
600
520
440
0
20
40
60
80
100
BOILING POINT
L.P. THEORY
H.P. THEORY
DATA

Fig 2

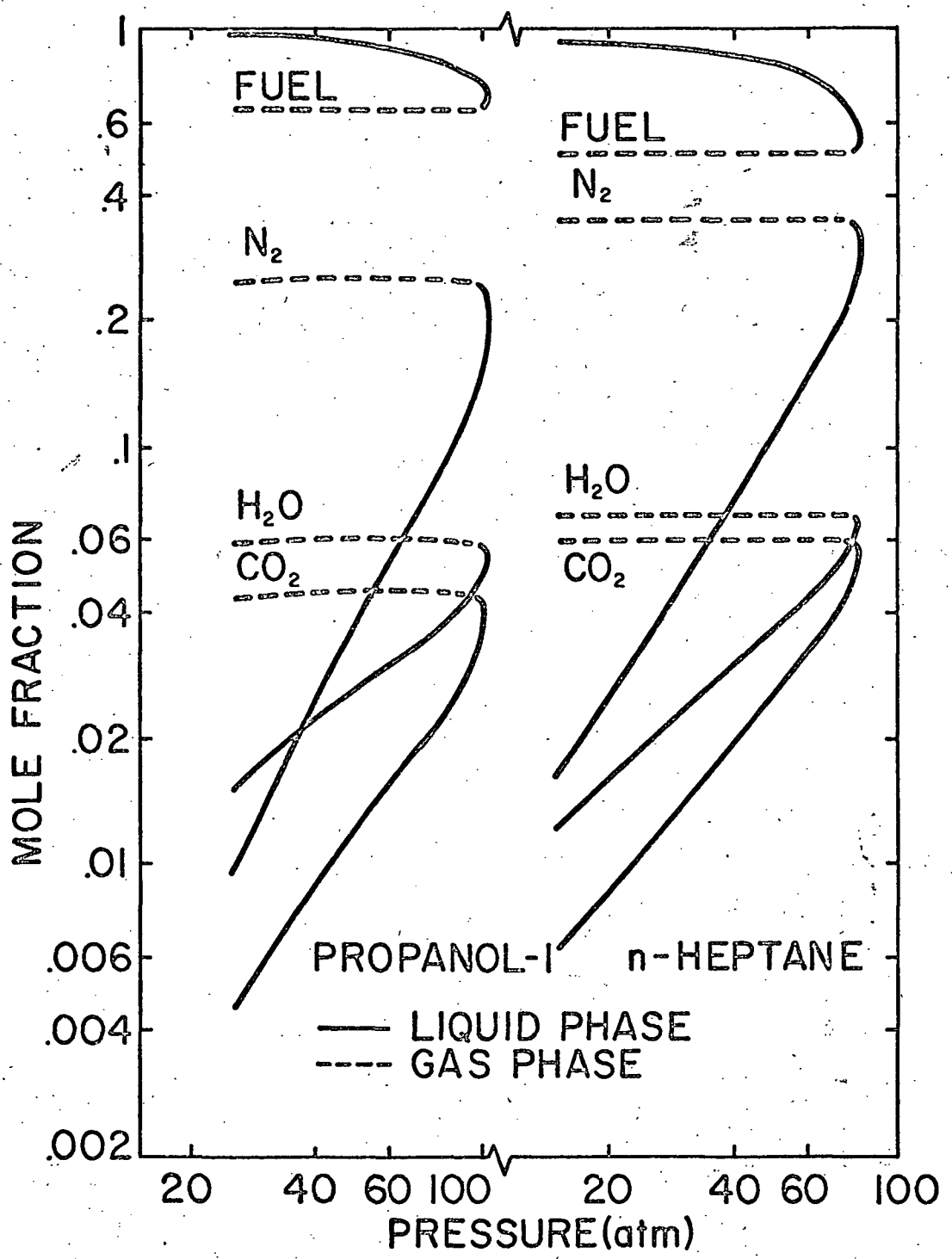
1
.6
.4
.2
.1
.06
.04
.02
.01
.006
.004
.002
MOLE FRACTION
FUEL
N2
H2O
CO2
FUEL
N2
H2O
CO2
PROPANOL-1
n-HEPTANE
LIQUID PHASE
GAS PHASE
20
40
60
100
20
40
60
100
PRESSURE(atm)